HHS Public Access

Author manuscript

J Immunol. Author manuscript; available in PMC 2024 April 01.

Published in final edited form as:

J Immunol. 2023 April 01; 210(7): 926–934. doi:10.4049/jimmunol.2200478.

miR-155 plays selective cell-intrinsic roles in brain infiltrating immune cell populations during neuroinflammation

Jacob W. Thompson[1], **Ruozhen Hu**[1], **Thomas B. Huffaker**[1], **Andrew G. Ramstead**[1], **H. Atakan Ekiz**[1], **Kaylyn M. Bauer**[1], **William W. Tang**[1], **Arevik Ghazaryan**[1], **June L. Round**[1,2], **Robert S. Fujinami**[1], **Ryan M. O'Connell**[1,2]

[1]Department of Pathology, Division of Microbiology and Immunology, University of Utah, Salt Lake City, UT 84112

[2]Hunstman Cancer Institute, University of Utah, Salt Lake City, UT 84112

Abstract

The pro-inflammatory microRNA-155 (miR-155) is highly expressed in the serum and CNS lesions of patients with multiple sclerosis (MS). Global knockout of miR-155 in mice confers resistance to a mouse model of MS, experimental autoimmune encephalomyelitis (EAE), by reducing the encephalogenic potential of CNS-infiltrating Th17 T cells. However, cell-intrinsic roles for miR-155 during EAE have not been formally determined. Here we utilize single-cell RNA sequencing and cell-specific conditional miR-155 knockouts to determine the importance of miR-155 expression in distinct immune cell populations. Time course single-cell sequencing revealed reductions in T cells, macrophages, and dendritic cells in global miR-155 knockout mice compared with wild-type controls at day 21 post EAE induction. Deletion of miR-155 in T cells, driven by CD4 Cre, significantly reduced disease severity similar to global miR-155 knockouts. CD11c Cre-mediated deletion of miR-155 in dendritic cells also resulted in a modest yet significant reduction in the development of EAE, with both T cell and dendritic cell-specific knockouts showing a reduction in Th17 T cell infiltration into the CNS. Although miR-155 is highly expressed in infiltrating macrophages during EAE, deletion of miR-155 using LysM Cre did not impact disease severity. Taken together, these data show that while miR-155 is highly expressed in most infiltrating immune cells, miR-155 has distinct roles and requirements depending on the cell type, and have done so using the gold-standard conditional knockout approach. This provides insights into which functionally relevant cell types should be targeted by the next generation of miRNA therapeutics.

Introduction

The injection of myelin peptide (MOG) with an adjuvant to induce experimental autoimmune encephalomyelitis (EAE) is known to be a clinically relevant murine model of multiple sclerosis (MS) [1]. Both EAE and MS are thought to be mediated by $CD4^+$ T cells and characterized by mononuclear cell infiltration into the CNS that promotes demyelination of white matter lesions [2]. In healthy individuals, the main $CD45^+$ immune

Corresponding author: Ryan M. O'Connell (ryan.oconnell@path.utah.edu).

cells present within the CNS are microglia and CNS-associated macrophages [3]. Upon induction of EAE, the diversity and complexity of the immune cell populations in the brain change drastically [4]. Dendritic cells and activated effector T cells cross the blood-brain barrier and express inflammatory cytokines, including IFN-γ and IL-17, which can damage neural tissue [1, 5–7]. The cytokines produced by the effector T cells can also recruit other damaging cell types to the CNS, such as monocytes, neutrophils, and γδ T cells, leading to even more myelin-sheath degradation. One possible mechanism underlying the T cell-mediated damage is the expression of microRNA-155 (miR-155), which is upregulated in MS and EAE [8, 9]. However, the exact cellular roles that miR-155 plays in MS are not fully understood, as T cells can be regulated by both cell-intrinsic and extrinsic mechanisms.

Presently, miR-155 is thought to contribute to the pathology of MS and has elevated expression in the lesions and peripheral blood mononuclear cells (PBMCs) of human MS patients [8, 10–12]. miR-155 is specifically expressed in hematopoietic cells and is known to play a critical role in hematopoietic cell development and function [13]. Overexpression of miR-155 has been associated with a variety of inflammatory disorders [14, 15]. Of note, mice deficient in miR-155 (miR-155$^{-/-}$) are highly resistant to EAE, showing decreased severity and delayed onset compared to wild-type (miR-155$^{+/+}$) controls [16, 17]. Anti-miR-155 treatment has also been shown to reduce clinical disease severity in mice [17]. The reduced EAE disease in miR-155 KO mice is due in part to a decrease in Th1 and Th17 T cell-mediated responses. Fewer Th1 and Th17 T cells lead to reduced IFN-γ and IL-17, which are known drivers of inflammation and EAE [18, 19]. LPS-treated dendritic cells from global miR-155 knockout mice have reduced expression of specific cytokines when activated *in vitro* that are required for inflammatory T cell development [16, 20]. While studies using global knockouts of miR-155 for EAE experiments have suggested many important cells and factors regulated by miR-155 and involved in disease progression, conditional deletion of miR-155 in vivo has not been utilized to directly test cell-intrinsic roles for miR-155 during neuroinflammatory diseases such as EAE.

To analyze differences in CNS infiltrating immune cell populations during EAE between wild-type and miR-155KO mice, we utilized 10X Genomics single-cell RNAseq (SCseq) over multiple time points to better understand how miR-155 impacts immune cell responses during EAE. This approach yielded a comprehensive view of miR-155-expressing cells, as well as the transcriptional changes in distinct immune cell types that are impacted by miR-155. Additionally, to better understand the role of miR-155 in specific cell subsets that were reduced in a miR-155-dependent manner by day 21, we studied the conditional deletion of miR-155 in T cells, macrophages, and dendritic cells using miR-155 floxed mice and relevant Cre driver strains. miR-155 is highly expressed in the T cell, monocyte, and dendritic cell compartments, and its expression in T cells, and to a lesser degree dendritic cells, clearly regulated their inflammatory status and selectively impacted their capacity to promote disease severity in the context of EAE. Determining the role of miR-155 in specific cell types will allow for a better understanding of the cell-intrinsic vs. extrinsic effects of miR-155 expression during the development of EAE, and will direct the design and development of future drugs that modulate miR-155 to treat MS.

Materials and Methods

Mice

All experiments were approved by the University of Utah Institutional Animal Care and Use Committee. Mice engineered to contain LoxP sites flanking miR-155 (miR-155$^{fl/fl}$) were crossed to mice expressing Cre under the control of the CD4 promoter (CD4 Cre) or the LysM promoter (LysM Cre) for T cell and myeloid cell-specific deletion of miR-155, with deletion confirmed as previously reported by our lab [21, 22]. For the novel dendritic cell-specific deletion of miR-155, miR-155$^{fl/fl}$ mice were crossed with CD11c-Cre-GFP mice, labeled as CD11c Cre, from Jackson Laboratory (Strain #:007567) that express Cre recombinase, an internal ribosomal entry site (IRES), and an enhanced green fluorescent protein (EGFP) downstream of the Itgax/CDllc promoter. miR-155$^{-/-}$, miR-155$^{+/+}$, miR-155$^{fl/fl}$, CD4 Cre, LysM Cre, CD11c Cre, and combinations of these mice are on a C57BL/6 genetic background. Groups of 6–14 age and sex-matched male and female mice, originally derived from littermates, with ages ranging from 8–13 weeks, were used in each experiment, and conditional knockout experiments were repeated at least two times.

Experimental Autoimmune Encephalomyelitis (EAE)

For induction of EAE, mice were injected subcutaneously (s.c.) into the base of the tail with a volume of 100 μl containing 100 μg/ml MOG35–55 peptide (BD Biosciences) emulsified in complete Freund's adjuvant (CFA), as we have described [16, 20]. Mice were also injected intraperitoneally (i.p). with 200 ng of pertussis toxin on days 0 and 2, and clinical symptoms were scored regularly according to the following criteria: 0, no symptoms; 0.5, partially limp tail; 1, completely limp tail; 1.5, impaired righting reflex; 2, hind limb paresis; 2.5, hind-limb paralysis; 3, forelimb weakness; 4, complete paralysis; 5, death.

miRNA isolation and quantitative real-time PCR

For confirmation of deletion of miR-155 in dendritic cells, CD11c^{+} splenic cells were enriched from CD11c-GFP-Cre^{+} miR-155$^{fl/fl}$ and control miR-155$^{fl/fl}$ mice by staining with fluorophore-conjugated anti-CD11c antibodies and sorting on a BD FACS Aria flow sorter (University of Utah Health Science Center). Total RNA was isolated with the Qiagen miRNeasy kit and expression of mature miR-155 and control U6 was determined with gene-specific primers from Exiqon run on an Applied Biosystems QuantStudio 6 Real-Time PCR instrument.

Single-cell RNA sequencing (scRNAseq)

Sample preparation and sequencing: Brain and spinal cord tissues were dissociated using scissors and forceps and processed on ice. After a percoll gradient, cells were stained with DAPI and APC-conjugated CD45 for 15 minutes on ice in PBS containing 2 mM EDTA and 0.5% BSA. Live CD45^{+} cells were sorted via BD FACSAria cell sorter and washed once in PBS containing 0.04% BSA. Samples were then processed for SCseq via a 10× platform according to the manufacturer's instructions (10× Genomics). Paired-end RNAseq (125 cycles) was performed via an Agilent HiSeq next-generation

sequencer. Sequencing reads were processed by using 10× Genomics CellRanger pipeline and further analyzed with the Seurat R package [23–26]. The effect of mitochondrial gene representation and the variance of unique molecular identifier (UMI) counts were regressed out from the data set prior to analysis. Gene expression signatures defining cell clusters were analyzed after aggregating 6 samples (miR-155$^{-/-}$ and miR-155+/+ at days 0, 13, and 21). The raw data from SCseq experiments in this manuscript can be found in the NCBI's Gene Expression Omnibus database (GSE206056 https://www.ncbi.nlm.nih.gov/geo/).

Identification of cell clusters: Cells in our dataset were clustered by using the FindClusters function of the Seurat analysis package, which identifies clusters via a shared nearest neighbor (SNN) modularity optimization-based algorithm. This function identified 22 distinct clusters spanning the lymphoid and myeloid cell lineages. Clusters were pooled into similar cell types and analyzed throughout the manuscript. The biological identities of cell clusters were annotated with the help of an immune-cell scoring algorithm (developed in-house and available at http://labs.path.utah.edu/oconnell/resources.htm) and by surveying known immune cell markers in the SCseq data set as previously described [23, 24]. Upon naming the clusters, the Seurat R package was used to create plots for the expression of selected genes. GSEA analysis was performed by using fgsea R package, after ranking genes using a signal-to-noise metric [27, 28].

Intracellular staining and flow cytometry

Cells were filtered through a 0.45-μm nylon filter to obtain single-cell suspensions. Cells were stained in Hank's balanced salt solution (HBSS) supplemented with 0.5% BSA and 2 mM EDTA by using the following fluorophore-conjugated antibodies (purchased from Biolegend or eBioscience/ThermoFisher Scientific): anti-CD3e (clone 145–2C11) (Pacific Blue), anti-CD8a (clone 53–6.7) (APC), anti-CD4, anti-CD11c, anti-CD45 (clone 30-F11) (PE-Cy7), anti-CD11b (clone M1/70) (PerCp-Cy5.5), anti-F4/80 (clone BM8) (PE), anti-CD64, anti MHCII, anti-B220, anti-XCR1, anti-CD172, and anti-CD103 at 1:500 to 1:1,000 dilutions. To detect intracellular expression of IL-17A, IFN-γ, or FoxP3 in CD4+ T cells, brain and spinal cord cells (purified with Percoll) were first treated with 750 ng/ml ionomycin and 50 ng/ml phorbol myristate acetate (PMA) (Calbiochem) in the presence of 0.5 μl of GolgiPlug (BD Biosciences) for 4–5 hr at 37°C. Cells were subsequently stained with surface markers and then permeabilized and fixed in 100 μl of eBioscience Perm-Fix solution overnight at 4°C. Cells were washed once in perm wash buffer (eBioscience) and then stained with 0.3 μg of fluorophore-conjugated anti-IL-17A, IFN-γ, or FoxP3 (eBioscience) for 20 min at 4°C. After staining cell surface antigens on ice for 15 minutes, cells were washed and analyzed using a BD LSRFortessa flow cytometer. Data analysis was done using FlowJo (Tree Star) and GraphPad Prism software.

Neuropathology

Mice were euthanized, on day 21 post EAE induction, and perfused with phosphate-buffered saline, followed by 4% paraformaldehyde phosphate buffered solution (Sigma-Aldrich, St. Louis, MO). The brain, coronally divided into five slabs, and the spinal cord, transversely divided into 12 segments, were embedded in paraffin. Four-micrometer-thick sections were stained with Luxol fast blue for myelin visualization. Histological scoring was performed

as described by Tsunoda et. Al. 2001 [29]. Brain sections were scored for meningitis (0, no meningitis; 1, mild cellular infiltrates; 2, moderate cellular infiltrates; 3, severe cellular infiltrates), perivascular cuffing (0, no cuffing; 1, 1 to 10 lesions; 2, 11 to 20 lesions; 3, 21 to 30 lesions; 4, 31 to 40 lesions; 5, over 40 lesions), and demyelination (0, no demyelination; 1, mild demyelination; 2, moderate demyelination; 3, severe demyelination). Each score from the brain was combined for a maximum score of 11 per mouse. For scoring of spinal cord sections, each spinal cord segment was divided into four quadrants: the ventral funiculus, the dorsal funiculus, and each lateral funiculus. Any quadrant containing meningitis, perivascular cuffing, or demyelination was given a score of 1 in that pathological class. The total number of positive quadrants for each pathological class was determined and then divided by the total number of quadrants present on the slide and multiplied by 100 to give the percent involvement for each pathological class. An overall pathological score was also determined by giving a positive score if any pathology was present in the quadrant. This was also presented as the percent involvement.

GSEA

RNAseq expression values from miR-155$^{-/-}$ and miR-155$^{+/+}$ subpopulations were ranked by using a signal-to-noise metric [27]. Ranked gene lists were then analyzed for gene set enrichment by using the fgsea R package as previously described [23]. Gene sets used in these analyses were derived from the Molecular Signature Database (MSigDB) [30].

Statistical analysis

Clinical scores were analyzed for individual days using the Mann Whitney U test and overall disease curves differences were determined with a two-sample t-test comparing the area under the curve (AUC) for each. Weight scores were compared with 2-way ANOVA. Assessments qPCR and flow cytometry data were performed using 2-tailed Student's t-tests. Wilcoxon's test was used for analyzing gene expression in select SCseq clusters. Reported P values were corrected for multiple comparisons by the Holm-Sidak method. P values less than or equal to 0.05 were considered statistically significant throughout (*P ≤ 0.05, **P ≤ 0.01, ***P ≤ 0.001, ****P ≤ 0.0001).

Results

Single-cell mapping of CD45^{+} cells from WT and miR-155$^{-/-}$ mice during EAE

It is known that MicroRNA-155 (miR-155) is an important factor in driving experimental autoimmune encephalomyelitis (EAE) [16, 17, 20]. Mice lacking miR-155 have reduced autoimmune inflammation and are highly resistant to the EAE disease. We induced EAE in mouse global knockouts of miR-155 (miR-155$^{-/-}$) and corresponding WT controls and their disease scores were tracked for 21 days (Figure 1A). Consistent with previous literature, miR-155$^{-/-}$ mice had significantly reduced clinical disease scores compared to WT mice [16, 17]. Groups were evaluated on days 0, 13, and 21 corresponding to naïve mice, mice before disease score separation, and mice after the disease scores have separated and plateaued in clinical disease severity, respectively (Figure 1A). CD45^{+} and DAPI^{-} cells from brains at each time point were flow-sorted for single-cell analysis with the 10x genomics platform (Supplemental Figure 1), similar to our previous approach [23, 24, 26]. Single-cell

RNAseq data from all mice were passed through the Cell Ranger analysis pipeline and to the Seurat R toolkit for single-cell genomics. 22 individual cell clusters were found via unsupervised principal correlation analysis based on unique RNA expression profiles (Figure 1B). These clusters were mapped using a uniform manifold approximation and projection (UMAP) algorithm to visually display the similarities in gene expression between the clusters (Figure 1C). We utilized our Cluster Identity Predictor (CIPR) algorithm, which compares the cluster gene expression of multiple genes simultaneously to known expression datasets from the ImmGen database to initially assess the identities of each individual cluster (Supplemental Figure 2) [24]. We found three clusters of microglia (Microglia1, Microglia 2, and Microglia 3), three monocyte clusters [Monocytes, Monocyte ($Ly6c^+$ $MHCII^+$), and Nonclassical Monocytes], five distinct T cell populations ($CD4^+$ T cells, $CD4^+$ Effector T cells, Naïve $CD4^+$ T cells, $CD8^+$ T cells, and γδ-T cells), two B cell clusters (B Cells1, B Cells2), five granulocyte clusters (Neutrophils1, Neutrophils2, Basophils, Granulocyte, and Stem-Progenitors), one natural killer cell population (Natural Killer Cells), and three dendritic cell clusters (cDCs, migDCs, pDCs) (Figure 1C). Cell cluster identities were verified by analyzing the expression of known cellular markers (Supplemental Figure 2). Pooled clusters of Granulocytes, B Cells, Microglia, Monocytes, T cells, Dendritic cells, and Natural Killer Cells were utilized for downstream gene expression analysis (Supplemental Figure 3). These data demonstrate that scRNA-Seq can be used to define distinct immune cell types in the brain during EAE.

Splitting the cell clusters based on genotype and time point revealed distinct patterns of cell infiltration into the brain during EAE for WT and miR-$155^{-/-}$ mice (Figures 1D and 1E). The percentage of microglia among $CD45^+$ cells decreased at day 13 as the other infiltrating cells entered the CNS and can be seen returning to normal percentages in the miR-$155^{-/-}$ mice at day 21, yet were still decreased in WT controls (Figures 1D and 1E). T cell percentages increased in WT mice as the disease progressed with percentages similar to miR-$155^{-/-}$ mice at days 0 and 13, but t day 21, the miR-$155^{-/-}$ T cell numbers have returned to normal levels while the WT mice with higher disease scores have further increased numbers of T cells present (Figures 1D and 1E). Monocytes also showed a similar trend with a dramatic increase in the number of cells in the CNS as disease severity increased in both WT and miR-$155^{-/-}$, but only miR-$155^{-/-}$ mice returned to lower levels at day 21 (Figures 1D and 1E). Natural killer cells, B cells, and dendritic cells are more prevalent in the miR-$155^{-/-}$ groups at day 13 than their WT controls, yet dendritic cells were at lower levels in miR-$155^{-/-}$ by day 21 (Figures 1D and 1E). Granulocytes generally show reduced percentages in the miR-$155^{-/-}$ mice, with increases in both groups as EAE progresses (Figures 1D and 1E). Taken together, these data indicate that miR-155 broadly influences the makeup of the immunological landscape in the brain during EAE.

WT T cells, Dendritic cells, and Monocytes are more inflammatory than miR-$155^{-/-}$ cells in the CNS during EAE

We performed gene set enrichment analysis (GSEA) of all hallmark pathways and analyzed several representative inflammatory markers expressed by each pooled cell clusters: microglia, T cells, monocytes, dendritic cells, granulocytes, B cells, and natural killer cells at days 0, 13, and 21 post EAE induction (Supplementary Figure 4). A variety of cell

signaling and activation pathways were differentially regulated in distinct immune cells analyzed in the presence vs. absence of miR-155. As we observed a large reduction in T cells, monocytes, and dendritic cells in miR-155$^{-/-}$ mice at day 21 compared to miR-155$^{+/+}$ controls, with each implicated in disease regulation, we analyzed these cell populations further. WT T cells present in the brain at day 21 are more inflammatory according to the hallmark interferon-gamma response pathway than miR-155$^{-/-}$ cells (Figure 2A). These WT T cells have higher expression of *Ccl5*, *CD28*, *CD69*, *Gzmb*, and *Icos* but no difference in *CD44* expression compared to miR-155$^{-/-}$ T cells (Figure 2B). The pooled clusters of monocytes and dendritic cells both showed significantly higher expression of Hallmark Inflammatory Response genes in the WT versus knockout miR-155$^{-/-}$ mice at day 21 (Figures 2C and 2E). miR-155$^{-/-}$ monocytes had significantly reduced expression of *Ccl5*, *CD40*, *CD86*, *IL1b*, and *Stat5a* with no significant difference in *Tnf* (Figure 2D). Similarly, miR-155$^{-/-}$ dendritic cells also displayed a selective reduction in certain genes including *Ccl5*, *CD40*, and *Il1b* with no statistical difference in *CD86*, *Stat5a*, and *Tnf* compared to control dendritic cells (Figure 2F). Thus, miR-155 is a promoter of inflammatory gene programs expressed by a variety of distinct brain-infiltrating immune cell types with established roles in driving inflammation during EAE.

CD4^{+} cell-specific deletion of miR-155 leads to reduced Th17 and Th1 T cells in the CNS during EAE

As previous studies assessing global knockout of miR-155 in EAE have pointed to defects in the development of Th1 and Th17 cells, leading to reduced T cell-dependent tissue inflammation, we studied the effect of removing miR-155 specifically from the T cell compartment during EAE. Conditional deletion of miR-155 in T cells (mir-155 CD4KO) was achieved by utilizing mice where a floxed miR-155 is deleted in CD4^{+} and CD8^{+} T cells under the expression of a CD4-Cre [21]. Both CD4^{+} and CD8^{+} T cells share a common double-positive stage where they express both CD4 and CD8, and the CD4 expression at that stage leads to the permanent deletion of miR-155 from T cells derived from these double-positive cells. EAE was induced in adult miR-155 CD4KO mice, along with miR-155 floxed controls, CD4-Cre alone, and miR-155$^{-/-}$ mice. Similar to miR-155$^{-/-}$ mice, miR-155 CD4KO mice developed significantly reduced EAE disease compared to the floxed or Cre alone control mice (Figure 3A). At day 21, CD45^{+} cells were isolated from the brains of the experimental mice and expression of IFN-γ and IL-17A in CD45^{+} CD4^{+} cells was measured via flow cytometry (Figure 3B). Among the CD45^{+} CD4^{+} cells found in the brain, miR-155 CD4KO mice had reduced levels of Th1 and Th17 cells in this compartment (Figure 3C and 3D). Similar reductions in activated T cells were found within the spinal cords (Supplementary Figure 5A). Neuropathology scores were given to brain and spinal cord histology sections from miR-155 CD4KO mice and litter mate floxed only mice (Figure 3E and Supplementary Figure 5B) [29, 31]. We confirmed significantly reduced perivascular cuffing, demyelination, and overall pathology scoring in the brains of CD4KO mice compared to the controls and found similar results in the spinal cord sections analyzed (Figure 3E and Supplementary Figure 5B). These data point to a clear, cell-intrinsic role for T cell expressed miR-155 during EAE in mice.

LysM$^+$ cell-specific deletion of miR-155

miR-155 specific deletion driven by LysM-Cre (mir-155 LysMKO) was used in order to examine the effect of losing miR-155 in infiltrating macrophage during EAE, as this Cre driver has previously been shown to delete miR-155 expression in macrophages [22]. EAE was induced in miR-155 LysMKO, miR-155 floxed, and miR-155 Cre mice (mice described by Huffaker et al. JBC 2017) [22]. There was no significant difference in the severity of EAE disease scoring between the mir-155 LysMKO and their controls (Figure 4A). Flow cytometry analysis showed no difference in the percentage of brain-infiltrating macrophages or in their activation status (Figure 4B). Further, no changes were observed in the percentage of macrophages that were skewed towards either the MHCII^{high} or MHCII^{low} phenotype (Figure 4C). The total number of brain microglia remained unchanged upon deletion of miR-155 by LysM-Cre (Figure 4D). Inflammatory Th17 and Th1 T cell numbers are also unchanged in the LysMKO mice compared with their control counterparts (Figure 4E). Taken together, these data indicate that LysM$^+$ infiltrating monocytes and macrophages do not require miR-155 to modulate disease severity or inflammation during EAE.

Dendritic cell-specific knockout of miR-155 leads to reduced EAE disease

In order to determine the role of miR-155 expression within dendritic cells during EAE, we generated conditional miR-155 knockout mice by crossing floxed miR-155 mice (miR-155$^{fl/fl}$) with CD11c-Cre-GFP mice (CD11c Cre) from Jackson Laboratory that express Cre recombinase, an internal ribosomal entry site (IRES), and an enhanced green fluorescent protein (EGFP) downstream of the Itgax/CDllc promoter to generate CD11c Cre$^+$ miR-155$^{fl/fl}$ (CD11cKO) mice. Mice were genotyped for the presence of CD11c Cre according to the Jackson Laboratory's protocols, and this resulted in expected PCR products using agarose gel electrophoresis (Figure 5A). To confirm the deletion of miR-155 from CD11c-expressing cells, we isolated total RNA from sorted splenic CD11c$^+$ cells of CD11cKO and miR-155$^{fl/fl}$ mice. Quantitative real-time PCR was run with mature miR-155 specific primers and normalized to the expression of the housekeeping small RNA U6 to determine relative ΔCt values (Figure 5B). EAE was induced in CD11c Cre$^+$ miR-155$^{fl/fl}$ and age and sex-matched floxed only control mice, and clinical disease scoring as well as weights were tracked for 21 days. The CD11cKO mice had significantly reduced disease severity and lost less weight than the miR-155$^{fl/fl}$ mice (Figures 5C and 5D). We also found no difference in EAE disease severity in CD11c Cre$^+$ only mice compared with littermate controls (Supplementary Figure 6). IFN-γ and IL-17A expression by CD45$^+$ CD4$^+$ T cells was measured by flow cytometry in miR-155$^{fl/fl}$ controls and CD11cKO mice, and revealed a significant reduction in the total number of Th17 and Th1 T cells present in the brain at day 21 (Figure 5E). The number of CD45+ CD64- MHCII^{high} dendritic cells was also decreased in the CD11cKO brains at day 21. However, these dendritic cells expressed similar amounts of the inflammatory marker CD86 (Figure 5F). A more specific analysis of dendritic cell subsets showed that this difference was found in both cCD1 and cDC2 subtypes, including between CD103$^+$ and CD103$^-$ subsets of cDC1 cells (Figure 5G, 5H, 5I, and 5J). Thus, in addition to T cells, miR-155 functions within brain DCs to promote inflammatory T cell responses and EAE disease phenotypes.

Discussion

In this paper, we investigated the cell-specific roles of miR-155 in certain CNS-infiltrating immune cells during EAE and made several important findings. First, we utilized single-cell RNA sequencing to determine the global changes in cell proportions throughout EAE, and most interestingly, a large reduction in the number of T cells, myeloid cells, and dendritic cells was observed in the brains of miR-155$^{-/-}$ mice compared to wild-type controls on day 21 post-EAE induction. In addition to revealing these cell types, our GSEA analysis also indicates that miR-155 has broad and complex impacts on gene expression pattern in CNS immune cells during neuroinflammation. Second, we found that deletion of miR-155 selectively in the T cell compartment is sufficient to reduce EAE disease severity to levels similar to global knockout mice. Third, miR-155 expression in the LysM^{+} myeloid compartment was dispensable for EAE disease progression. Fourth, we determined that miR-155 expression in dendritic cells is needed for full EAE disease progression. These data, acquired through the use of conditional knockout mice, demonstrate that miR-155 has distinct roles depending on the cell type where it is being expressed, and is only required in a subset of infiltrating immune cells during EAE, and possibly MS.

Previous studies have shown that mice lacking miR-155 have reduced numbers of Th17 cells and that those Th17 cells are incapable of causing EAE disease to the same level as wild-type Th17 cells on a per-cell basis [20]. While it has previously been shown that miR-155 expression is important for effector gene expression in T cells, we were able to determine that specific deletion of miR-155 within the T cell compartment is sufficient to ameliorate EAE disease *in vivo*. This reduction in EAE development is thought to be due to miR-155 targeting multiple genes, especially Ets1, a well-established negative regulator of Th17 differentiation [20]. Our GSEA data presented here suggests that additional pathways in T cells, and possible T cell subtypes, are likely also involved in regulating this response, and warrant further exploration moving forward.

It was demonstrated some time ago that a large portion of the CNS infiltrating immune cells during EAE are peripheral myeloid-derived monocytes and macrophages [32]. miR-155 is thought to be involved in the MHCII^{high}/ MHCII^{low} polarization states of macrophages in other contexts, and depletion of these myeloid cells leads to protection against EAE [33–35]. Early in the disease, monocytes are activated to become MHCII^{high} macrophages which release reactive oxygen species that damage the myelin sheath surrounding neurons [36]. With the importance of monocytes in EAE disease progression combined with their high expression of miR-155, the lack of a phenotype with the LysM Cre-specific deletion of miR-155 during EAE is a surprising result that shows a previously unappreciated specificity for the cellular requirement for miR-155 during EAE, yet we do not rule out roles for macrophage expressed miR-155 in other biological contexts. Of note is our observation that, while not statistically significant, LysM-specific deletion of miR-155 may result in a small change in the onset of disease, with the Cre-deleted animals possibly developing disease symptoms earlier than the control animals. Further, LysM^{-} monocytes and macrophages may also utilize miR-155 during neuroinflammation, and can be examined in future work.

Dendritic cells have been shown to play a number of important roles in the progression of EAE [37]. While originally thought to be absent in the CNS, small populations exist in the uninjured CNS and the number of dendritic cells greatly increases during the course of EAE. $CD11c^+$ dendritic cells are the main antigen-presenting cells during EAE, and increasing the number of DCs leads to worse EAE disease [5–7, 38]. Mice lacking H2-Ab1 on $CD11c^+$ cells have reduced antigen-specific T cell activation and are protected from severe EAE [4, 5]. Similarly, we see that depleting miR-155 from DCs results in reduced Th17 cells in the CNS along with reduced disease scores. The subset of DCs involved in this phenotype may also be narrowed down further as up to forty percent of the CD103+ DCs are also targeted with the LysM-Cre that we have shown has no effect on disease severity [39]. Although microglia express miR-155 and can upregulate CD11c upon activation, studies have shown that these CNS-resident cells do not present the MOG peptide *in vivo* [5, 40, 41]. This reduction in disease may be caused by several mechanisms, such as a reduction in total inflammatory DCs present in the CNS during EAE, a reduction in the inflammatory cytokines produced, such as IL-1β known to instruct Th17 responses, or fewer inflammatory extracellular vesicles. As inflammatory dendritic cells are known to release large numbers of extracellular vesicles that contain functional miR-155, it is possible that the reduction in EAE severity in CD11cKO mice is also due to the loss of inflammatory cargo in these vesicles [42]. Further clarifying the mechanisms by which miR-155 within dendritic cells regulates neuroinflammation will be a focus of future investigation.

Taken together, our work points to significant, cell-intrinsic roles for miR-155 in T cells and, to a lesser degree, dendritic cells during EAE disease in mice, which is the first demonstration of cell intrinsic functions for miR-155 using conditional knockout mice, to our knowledge. This information not only informs our understanding of miR-155's roles during inflammation, but also points to key cell types where its therapeutic targeting could be utilized in the treatment of MS patients.

Supplementary Material

Refer to Web version on PubMed Central for supplementary material.

Acknowledgments

This work was supported by an NMSS collaborative center grant (RMO and JLR) and an NINDS T32 training grant 5T32NS115664–02 (JLT). We also thank the University of Utah Flow Cytometry and Gene Expression Core Facilities.

References

1. Lock C, Hermans G, Pedotti R, Brendolan A, Schadt E, Garren H, Langer-Gould A, Strober S, Cannella B, Allard J, Klonowski P, Austin A, Lad N, Kaminski N, Galli SJ, Oksenberg JR, Raine CS, Heller R, and Steinman L, Gene-microarray analysis of multiple sclerosis lesions yields new targets validated in autoimmune encephalomyelitis. Nat Med, 2002. 8(5): p. 500–8. [PubMed: 11984595]
2. Dendrou CA, Fugger L, and Friese MA, Immunopathology of multiple sclerosis. Nat Rev Immunol, 2015. 15(9): p. 545–58. [PubMed: 26250739]
3. Hammond TR, Dufort C, Dissing-Olesen L, Giera S, Young A, Wysoker A, Walker AJ, Gergits F, Segel M, Nemesh J, Marsh SE, Saunders A, Macosko E, Ginhoux F, Chen J, Franklin RJM, Piao

X, McCarroll SA, and Stevens B, Single-Cell RNA Sequencing of Microglia throughout the Mouse Lifespan and in the Injured Brain Reveals Complex Cell-State Changes. Immunity, 2019. 50(1): p. 253–271 e6. [PubMed: 30471926]

4. Jordao MJC, Sankowski R, Brendecke SM, Sagar G. Locatelli, Tai YH, Tay TL, Schramm E, Armbruster S, Hagemeyer N, Gross O, Mai D, Cicek O, Falk T, Kerschensteiner M, Grun D, and Prinz M, Single-cell profiling identifies myeloid cell subsets with distinct fates during neuroinflammation. Science, 2019. 363(6425).
5. Greter M, Heppner FL, Lemos MP, Odermatt BM, Goebels N, Laufer T, Noelle RJ, and Becher B, Dendritic cells permit immune invasion of the CNS in an animal model of multiple sclerosis. Nat Med, 2005. 11(3): p. 328–34. [PubMed: 15735653]
6. Miller SD, McMahon EJ, Schreiner B, and Bailey SL, Antigen presentation in the CNS by myeloid dendritic cells drives progression of relapsing experimental autoimmune encephalomyelitis. Ann N Y Acad Sci, 2007. 1103: p. 179–91. [PubMed: 17376826]
7. Mundt S, Mrdjen D, Utz SG, Greter M, Schreiner B, and Becher B, Conventional DCs sample and present myelin antigens in the healthy CNS and allow parenchymal T cell entry to initiate neuroinflammation. Sci Immunol, 2019. 4(31).
8. Junker A, Krumbholz M, Eisele S, Mohan H, Augstein F, Bittner R, Lassmann H, Wekerle H, Hohlfeld R, and Meinl E, MicroRNA profiling of multiple sclerosis lesions identifies modulators of the regulatory protein CD47. Brain, 2009. 132(Pt 12): p. 3342–52. [PubMed: 19952055]
9. McCoy CE, miR-155 Dysregulation and Therapeutic Intervention in Multiple Sclerosis. Adv Exp Med Biol, 2017. 1024: p. 111–131. [PubMed: 28921467]
10. Noorbakhsh F, Ellestad KK, Maingat F, Warren KG, Han MH, Steinman L, Baker GB, and Power C, Impaired neurosteroid synthesis in multiple sclerosis. Brain, 2011. 134(Pt 9): p. 2703–21. [PubMed: 21908875]
11. Moore CS, Rao VT, Durafourt BA, Bedell BJ, Ludwin SK, Bar-Or A, and Antel JP, miR-155 as a multiple sclerosis-relevant regulator of myeloid cell polarization. Ann Neurol, 2013. 74(5): p. 709–20. [PubMed: 23818336]
12. Paraboschi EM, Solda G, Gemmati D, Orioli E, Zeri G, Benedetti MD, Salviati A, Barizzone N, Leone M, Duga S, and Asselta R, Genetic association and altered gene expression of mir-155 in multiple sclerosis patients. Int J Mol Sci, 2011. 12(12): p. 8695–712. [PubMed: 22272099]
13. Landgraf P, Rusu M, Sheridan R, Sewer A, Iovino N, Aravin A, Pfeffer S, Rice A, Kamphorst AO, Landthaler M, Lin C, Socci ND, Hermida L, Fulci V, Chiaretti S, Foa R, Schliwka J, Fuchs U, Novosel A, Muller RU, Schermer B, Bissels U, Inman J, Phan Q, Chien M, Weir DB, Choksi R, De Vita G, Frezzetti D, Trompeter HI, Hornung V, Teng G, Hartmann G, Palkovits M, Di Lauro R, Wernet P, Macino G, Rogler CE, Nagle JW, Ju J, Papavasiliou FN, Benzing T, Lichter P, Tam W, Brownstein MJ, Bosio A, Borkhardt A, Russo JJ, Sander C, Zavolan M, and Tuschl T, A mammalian microRNA expression atlas based on small RNA library sequencing. Cell, 2007. 129(7): p. 1401–14. [PubMed: 17604727]
14. Vigorito E, Kohlhaas S, Lu D, and Leyland R, miR-155: an ancient regulator of the immune system. Immunol Rev, 2013. 253(1): p. 146–57. [PubMed: 23550644]
15. Seddiki N, Brezar V, Ruffin N, Levy Y, and Swaminathan S, Role of miR-155 in the regulation of lymphocyte immune function and disease. Immunology, 2014. 142(1): p. 32–8. [PubMed: 24303979]
16. O'Connell RM, Kahn D, Gibson WS, Round JL, Scholz RL, Chaudhuri AA, Kahn ME, Rao DS, and Baltimore D, MicroRNA-155 promotes autoimmune inflammation by enhancing inflammatory T cell development. Immunity, 2010. 33(4): p. 607–19. [PubMed: 20888269]
17. Murugaiyan G, Beynon V, Mittal A, Joller N, and Weiner HL, Silencing microRNA-155 ameliorates experimental autoimmune encephalomyelitis. J Immunol, 2011. 187(5): p. 2213–21. [PubMed: 21788439]
18. Bettelli E, Carrier Y, Gao W, Korn T, Strom TB, Oukka M, Weiner HL, and Kuchroo VK, Reciprocal developmental pathways for the generation of pathogenic effector TH17 and regulatory T cells. Nature, 2006. 441(7090): p. 235–8. [PubMed: 16648838]

19. Ivanov II, McKenzie BS, Zhou L, Tadokoro CE, Lepelley A, Lafaille JJ, Cua DJ, and Littman DR, The orphan nuclear receptor RORgammat directs the differentiation program of proinflammatory IL-17+ T helper cells. Cell, 2006. 126(6): p. 1121–33. [PubMed: 16990136]
20. Hu R, Huffaker TB, Kagele DA, Runtsch MC, Bake E, Chaudhuri AA, Round JL, and O'Connell RM, MicroRNA-155 confers encephalogenic potential to Th17 cells by promoting effector gene expression. J Immunol, 2013. 190(12): p. 5972–80. [PubMed: 23686497]
21. Hu R, Kagele DA, Huffaker TB, Runtsch MC, Alexander M, Liu J, Bake E, Su W, Williams MA, Rao DS, Moller T, Garden GA, Round JL, and O'Connell RM, miR-155 promotes T follicular helper cell accumulation during chronic, low-grade inflammation. Immunity, 2014. 41(4): p. 605–19. [PubMed: 25367574]
22. Huffaker TB, Lee SH, Tang WW, Wallace JA, Alexander M, Runtsch MC, Larsen DK, Thompson J, Ramstead AG, Voth WP, Hu R, Round JL, Williams MA, and O'Connell RM, Antitumor immunity is defective in T cell-specific microRNA-155-deficient mice and is rescued by immune checkpoint blockade. J Biol Chem, 2017. 292(45): p. 18530–18541. [PubMed: 28912267]
23. Ekiz HA, Huffaker TB, Grossmann AH, Stephens WZ, Williams MA, Round JL, and O'Connell RM, MicroRNA-155 coordinates the immunological landscape within murine melanoma and correlates with immunity in human cancers. JCI Insight, 2019. 4(6).
24. Ekiz HA, Conley CJ, Stephens WZ, and O'Connell RM, CIPR: a web-based R/shiny app and R package to annotate cell clusters in single cell RNA sequencing experiments. BMC Bioinformatics, 2020. 21(1): p. 191. [PubMed: 32414321]
25. Ramstead AG, Wallace JA, Lee SH, Bauer KM, Tang WW, Ekiz HA, Lane TE, Cluntun AA, Bettini ML, Round JL, Rutter J, and O'Connell RM, Mitochondrial Pyruvate Carrier 1 Promotes Peripheral T Cell Homeostasis through Metabolic Regulation of Thymic Development. Cell Rep, 2020. 30(9): p. 2889–2899 e6. [PubMed: 32130894]
26. Huffaker TB, Ekiz HA, Barba C, Lee SH, Runtsch MC, Nelson MC, Bauer KM, Tang WW, Mosbruger TL, Cox JE, Round JL, Voth WP, and O'Connell RM, A Stat1 bound enhancer promotes Nampt expression and function within tumor associated macrophages. Nat Commun, 2021. 12(1): p. 2620. [PubMed: 33976173]
27. Subramanian A, Tamayo P, Mootha VK, Mukherjee S, Ebert BL, Gillette MA, Paulovich A, Pomeroy SL, Golub TR, Lander ES, and Mesirov JP, Gene set enrichment analysis: a knowledge-based approach for interpreting genome-wide expression profiles. Proc Natl Acad Sci U S A, 2005. 102(43): p. 15545–50. [PubMed: 16199517]
28. Gennady Korotkevich VS, Nikolay Budin, Boris Shpak, Maxim N. Artyomov, Alexey Sergushichev, Fast gene set enrichment analysis. bioRxiv, 2021.
29. Tsunoda I, Wada Y, Libbey JE, Cannon TS, Whitby FG, and Fujinami RS, Prolonged gray matter disease without demyelination caused by Theiler's murine encephalomyelitis virus with a mutation in VP2 puff B. J Virol, 2001. 75(16): p. 7494–505. [PubMed: 11462022]
30. Liberzon A, A description of the Molecular Signatures Database (MSigDB) Web site. Methods Mol Biol, 2014. 1150: p. 153–60. [PubMed: 24743996]
31. Tsunoda I, Tanaka T, and Fujinami RS, Regulatory role of CD1d in neurotropic virus infection. J Virol, 2008. 82(20): p. 10279–89. [PubMed: 18684818]
32. Huitinga I, van Rooijen N, de Groot CJ, Uitdehaag BM, and Dijkstra CD, Suppression of experimental allergic encephalomyelitis in Lewis rats after elimination of macrophages. J Exp Med, 1990. 172(4): p. 1025–33. [PubMed: 2145387]
33. Tran EH, Hoekstra K, van Rooijen N, Dijkstra CD, and Owens T, Immune invasion of the central nervous system parenchyma and experimental allergic encephalomyelitis, but not leukocyte extravasation from blood, are prevented in macrophage-depleted mice. J Immunol, 1998. 161(7): p. 3767–75. [PubMed: 9759903]
34. O'Connell RM, Taganov KD, Boldin MP, Cheng G, and Baltimore D, MicroRNA-155 is induced during the macrophage inflammatory response. Proc Natl Acad Sci U S A, 2007. 104(5): p. 1604–9. [PubMed: 17242365]
35. O'Neill LA, Sheedy FJ, and McCoy CE, MicroRNAs: the fine-tuners of Toll-like receptor signalling. Nat Rev Immunol, 2011. 11(3): p. 163–75. [PubMed: 21331081]

36. Nikic I, Merkler D, Sorbara C, Brinkoetter M, Kreutzfeldt M, Bareyre FM, Bruck W, Bishop D, Misgeld T, and Kerschensteiner M, A reversible form of axon damage in experimental autoimmune encephalomyelitis and multiple sclerosis. Nat Med, 2011. 17(4): p. 495–9. [PubMed: 21441916]

37. Matyszak MK and Perry VH, The potential role of dendritic cells in immune-mediated inflammatory diseases in the central nervous system. Neuroscience, 1996. 74(2): p. 599–608. [PubMed: 8865208]

38. Giles DA, Duncker PC, Wilkinson NM, Washnock-Schmid JM, and Segal BM, CNS-resident classical DCs play a critical role in CNS autoimmune disease. J Clin Invest, 2018. 128(12): p. 5322–5334. [PubMed: 30226829]

39. McCubbrey AL, Allison KC, Lee-Sherick AB, Jakubzick CV, and Janssen WJ, Promoter Specificity and Efficacy in Conditional and Inducible Transgenic Targeting of Lung Macrophages. Front Immunol, 2017. 8: p. 1618. [PubMed: 29225599]

40. Cardoso AL, Guedes JR, Pereira de Almeida L, and Pedroso de Lima MC, miR-155 modulates microglia-mediated immune response by down-regulating SOCS-1 and promoting cytokine and nitric oxide production. Immunology, 2012. 135(1): p. 73–88. [PubMed: 22043967]

41. Freilich RW, Woodbury ME, and Ikezu T, Integrated expression profiles of mRNA and miRNA in polarized primary murine microglia. PLoS One, 2013. 8(11): p. e79416. [PubMed: 24244499]

42. Alexander M, Hu R, Runtsch MC, Kagele DA, Mosbruger TL, Tolmachova T, Seabra MC, Round JL, Ward DM, and O'Connell RM, Exosome-delivered microRNAs modulate the inflammatory response to endotoxin. Nat Commun, 2015. 6: p. 7321. [PubMed: 26084661]

Key Points

1. miR-155 has a broad impact on the brain's immunological landscape during EAE
2. miR-155 regulates both immune cell dynamics and gene expression in the brain
3. miR-155 plays cell intrinsic functional roles in brain T cells and DCs during EAE

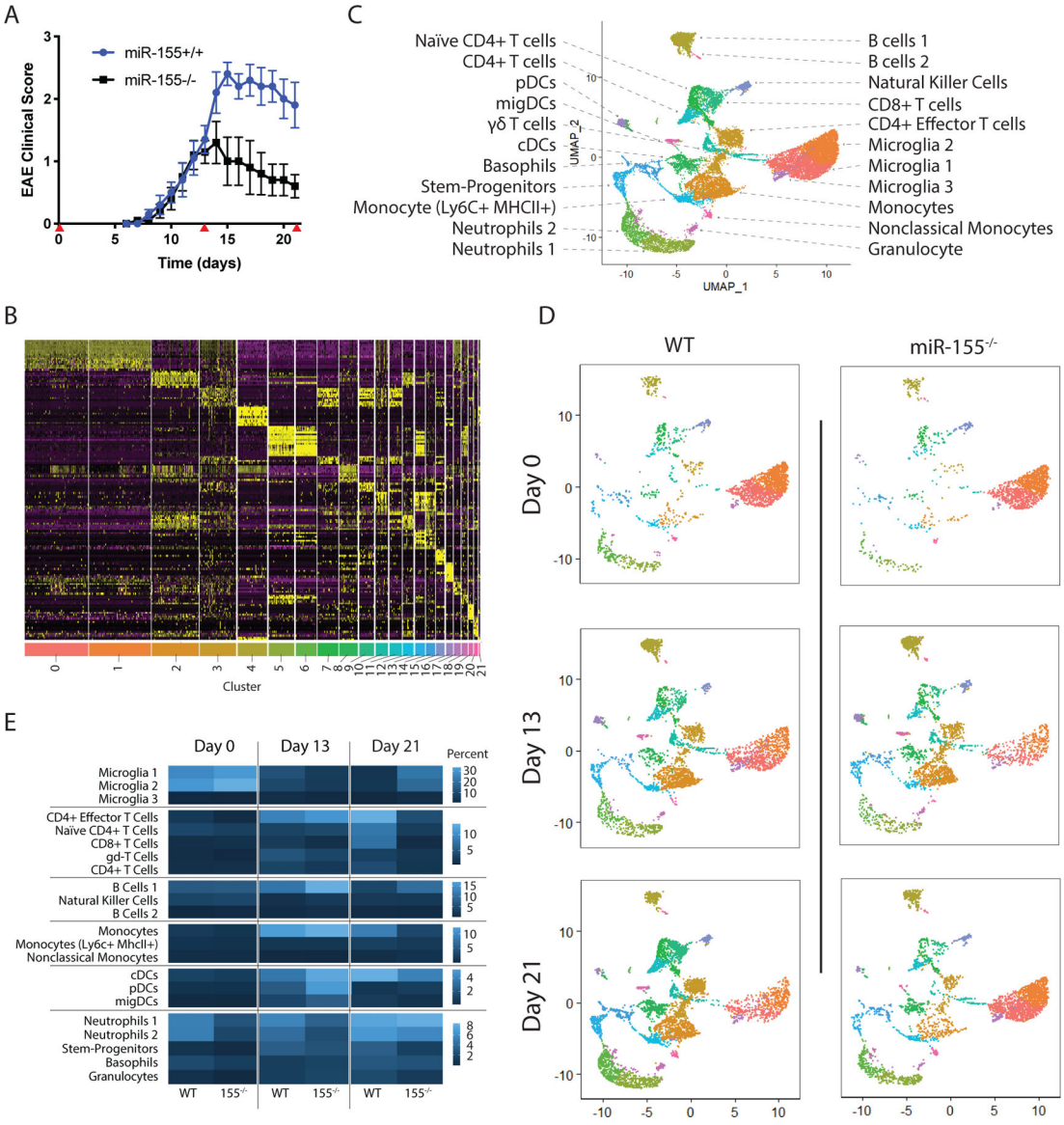

Figure 1. miR-155 deletion leads to altered CD45+ immune cell populations in mouse brains during EAE according to RNA SCseq.

A. EAE was induced in miR-155$^{+/+}$ and miR-155$^{-/-}$ mice by immunizing both groups with 100 μg of the $MOG_{35–55}$ peptide followed by administration of pertussis toxin. Their disease severity was scored daily based on clinical symptoms (n = 15). Red triangles indicate harvest time points of at day 0, day 13, and day 21 (n = 5 per day) of CD45^{+} cells from the brain for SCseq. B. Gene expression heat map showing top differentially expressed genes in clusters. Columns indicate individual cells grouped into 22 clusters and rows indicate genes. The column widths are proportional to the numbers of cells in clusters. C. Uniform Manifold Approximation and Projection (UMAP) plot of SCseq data showing 22 distinct clusters (aggregate data from miR-155$^{+/+}$ and miR-155$^{-/-}$ samples from days 0, 13, and 21). Cluster labels based on CIPR, an immune-cell scoring algorithm developed in-house. D. UMAP plots divided into individual miR-155$^{+/+}$ and miR-155$^{-/-}$ samples from days 0, 13, and 21. E. Heatmap showing quantification of the percentage that each cluster represents

for the total $CD45^+$ population in the brain for each genotype, separated by day of analysis. Scale of each group of clusters is shown to the right of each.

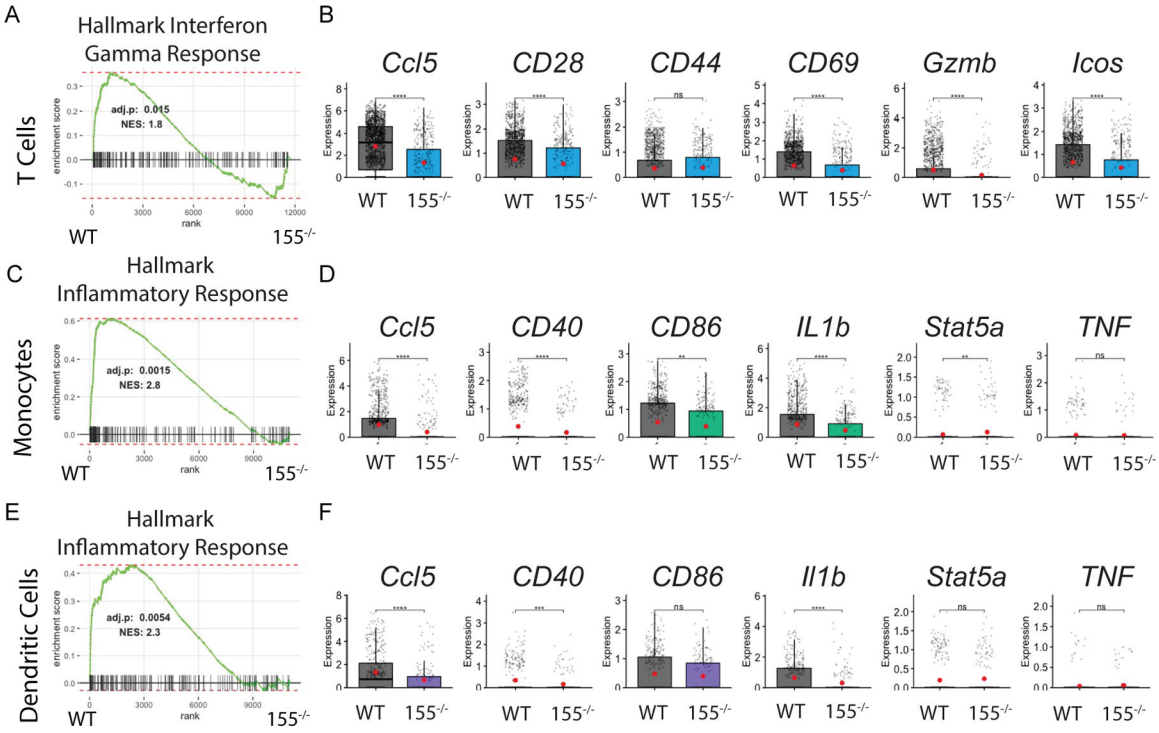

Figure 2. T cells, monocytes, and dendritic cells in the brains of miR-155$^{-/-}$ mice are less inflammatory than miR-155$^{+/+}$ cells at day 21 post-EAE

A. GSEA for Hallmark interferon-gamma response showing enrichment of genes in miR-155$^{+/+}$ compared with miR-155$^{-/-}$ samples. B. Differential expression analysis of a subset of T cell inflammatory marker genes: Ccl5, CD28, CD44, CD69, Gzmb, and Icos respectively. Each dot represents a single cell. Normalized expression values were used, and random noise was added to show distribution of data points. The box plots show interquartile range and the median value (bold horizontal bar). Average expression value per sample is indicated by the red points. Wilcoxon's test was used for statistical comparisons. *P ≤ 0.05, **P ≤ 0.01, ***P ≤ 0.001, ****P ≤ 0.0001; ns, P > 0.05. C. GSEA for Hallmark inflammatory response genes from SCseq data of all pooled monocyte clusters from day 21, showing enrichment of genes in miR-155$^{+/+}$ compared with miR-155$^{-/-}$ samples. D. Differential expression analysis of monocyte activation markers. Ccl5, CD40, CD86, IL1b, Stat5a, and TNF respectively. Data represented as described in B. E. GSEA for Hallmark inflammatory response genes from SCseq data of all pooled dendritic cell clusters from day 21, showing enrichment of genes in miR-155$^{+/+}$ compared with miR-155$^{-/-}$ samples. F. Differential expression analysis of dendritic cell activation markers. Ccl5, CD40, CD86, IL1b, Stat5a, and TNF respectively. Data represented as described in B.

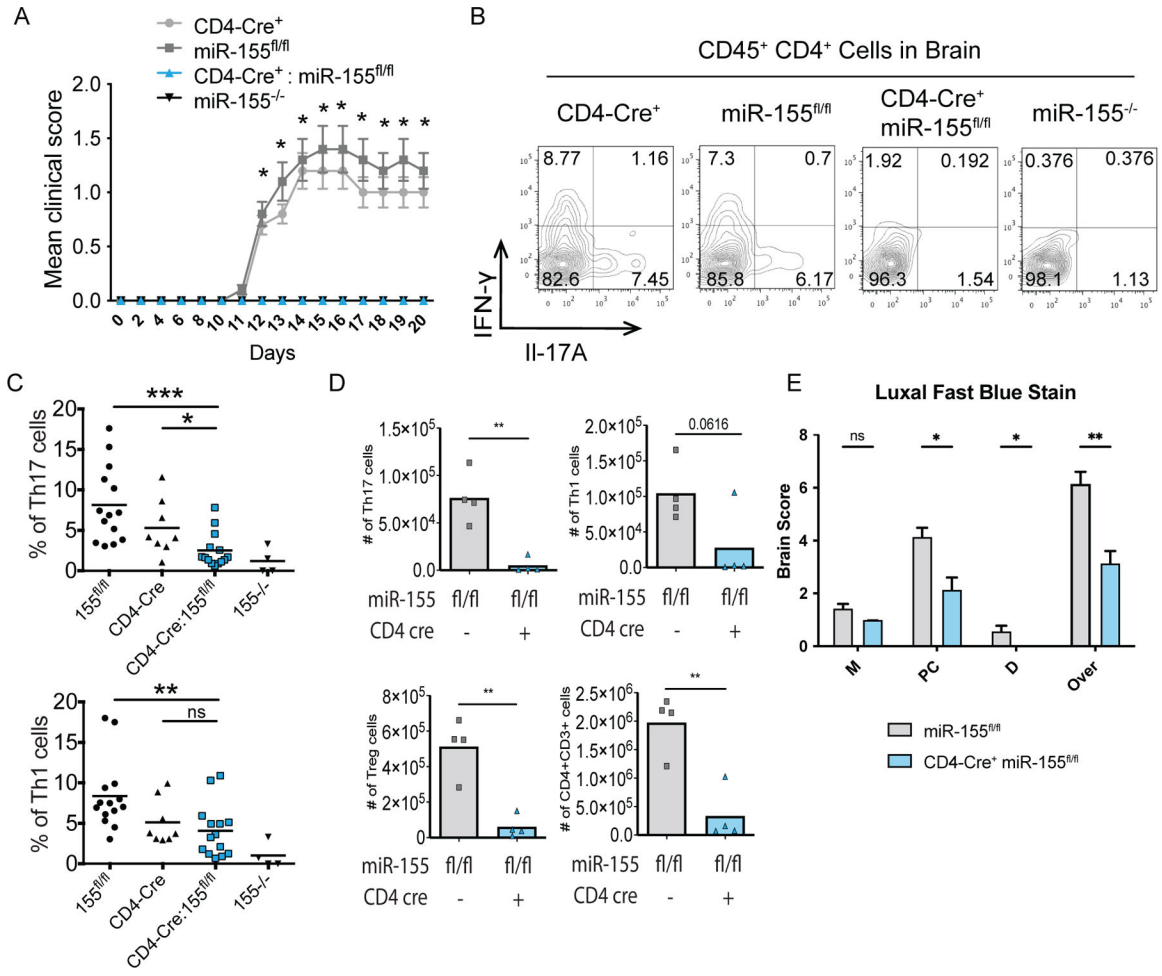

Figure 3. Conditional deletion of miR-155 in T cells by CD4 Cre leads to amelioration of EAE disease severity

A. EAE was induced in CD4-Cre^{+}, miR-155$^{fl/fl}$, CD4-Cre^{+} miR-155$^{fl/fl}$, and miR-155$^{-/-}$ mice by immunizing groups with 100 μg of the $MOG_{35–55}$ peptide followed by administration of pertussis toxin. Their disease severity was scored daily based on clinical symptoms (n = 8). B. Intracellular cytokine staining was conducted to identify total brain CD45^{+} CD4^{+} lymphocytes producing IL-17A and or IFN-γ. Transcription factor labeling for FoxP3 was also used to identify populations of Tregs in the CD45^{+} CD4^{+} T cells. C. Average percentage of CD45+ CD4+ cells in the brain at day 21 producing IL-17A or IFN-γ. Each dot represents a single mouse, average percentage represented by a horizontal bar. Chi-squared test was used for statistical comparisons. *P ≤ 0.05, **P ≤ 0.01, ***P ≤ 0.001; ns, P > 0.05. D. Total number of Th17, Th1, Treg, and total CD4+ T cells in the brains of mice at day 21 post EAE induction (n = 4). Average shown as box, individual mouse values shown as dots and triangles respectively. Student's t-test was used for statistical comparisons. *P ≤ 0.05, **P ≤ 0.01, ***P ≤ 0.001, ****P ≤ 0.0001, or numerical p value shown. E. Meningitis (M), perivascular cuffing (PC), demyelination (D), and overall brain pathology scores for mice sacrificed on day 21 post EAE. Data is given as the mean + SEM for groups of 7 mice. * P<0.05, Mann-Whitney U test.

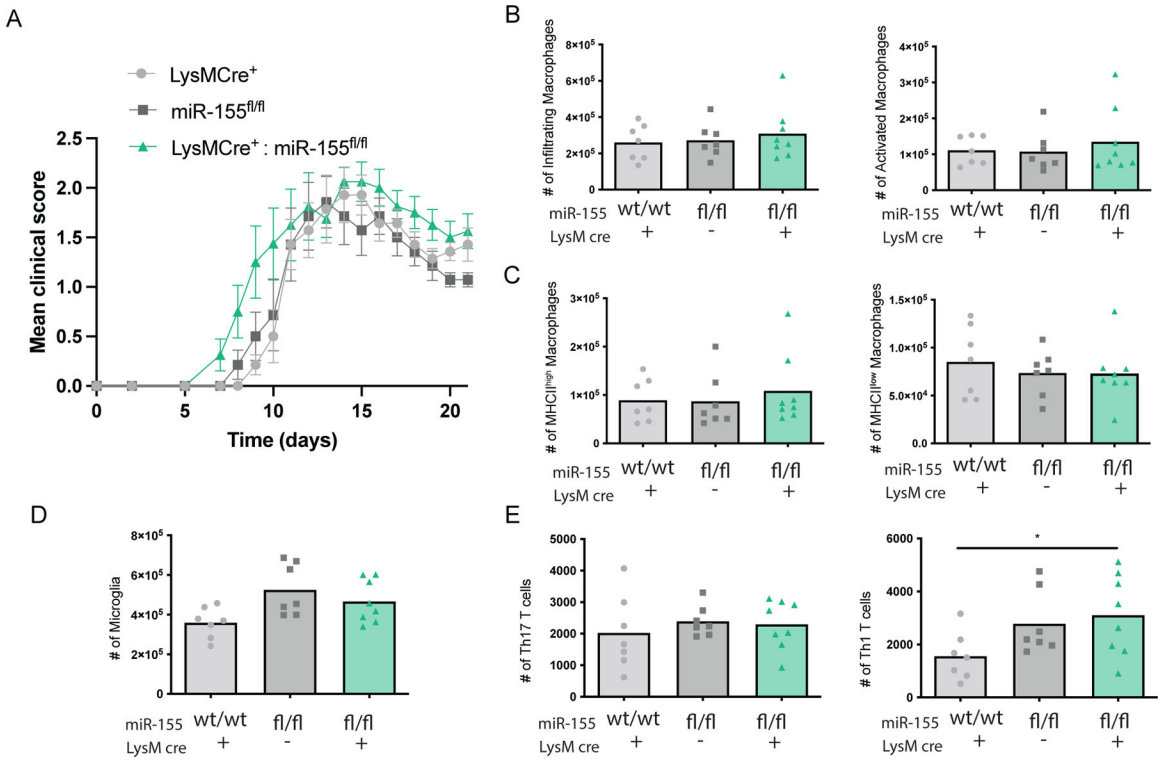

Figure 4. Conditional deletion of miR-155 by LysM Cre does not impact EAE disease severity or immune cell infiltration into the brain

LysM-Cre^{+}, miR-155$^{fl/fl}$, and CD4-Cre^{+} miR-155$^{fl/fl}$ brains were harvested on day 21 after immunizing with 100 μg of the $MOG_{35–55}$ peptide followed by administration of pertussis toxin. A. Disease severity as a mean clinical score is shown. Animals were scored daily based on clinical symptoms (n = 7–8). B. Total number of infiltrating macrophages and activated macrophages in the brain at day 21 post-EAE based on CD45^{high} CD11b^{+} F4/80^{+} and the number of those macrophages who also stained CD86^{+} respectively (n = 7–8). C. Total number of macrophages based on MHCII^{high} or MHCII^{low} staining of CD45^{high} CD11b^{+} F4/80^{+} Ly6c^{low} cells in the brain (n = 7–8). D. Brain microglia numbers (n = 7–8). E. Intracellular staining was used to determine the total number of Th17 and Th1 cells in the brain (n = 7–8).

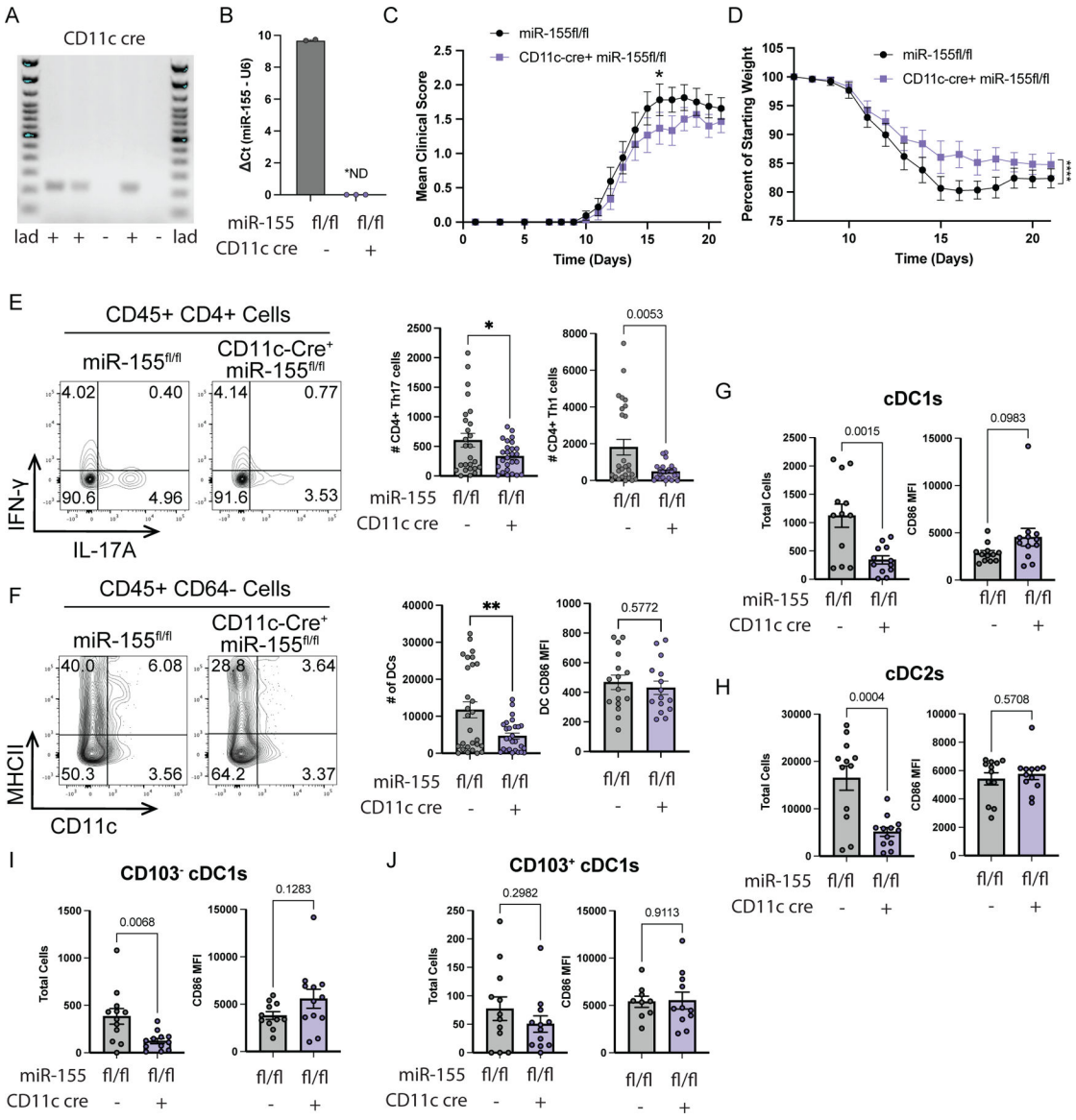

Figure 5. Deletion of miR-155 by in CD11c expressing cells leads to reduced EAE disease and inflammatory immune cells in the brain

CD11c Cre^{+} miR-155$^{fl/fl}$ mice were generated and EAE induced. Mice brains were harvested after 21 days. A. PCR amplification of CD11c Cre from ear punch DNA of miR-155$^{fl/fl}$ mice B. Relative expression of miR-155 in sorted splenic CD11c^{+} cells from naïve CD11c Cre^{+} miR-155$^{fl/fl}$ and CD11c Cre^{-} miR-155$^{fl/fl}$ mice. Circles show ratio of miR-155 to U6. *ND = no miR-155 was detectable in CD11c Cre^{+} miR-155$^{fl/fl}$ samples. C. $MOG_{35–55}$-induced EAE was induced in miR-155$^{fl/fl}$ mice, with and without the presence of CD11c Cre and disease was scored daily for 21 days. Graph represents pooled data from two separate experiments. D. Percent weight loss data from experiments described in C. E. Representative flow plot and quantification of Th17 and Th1 cells determined by intracellular staining to identify total number of CD45+ CD4+ cells producing IL-17A and/or IFN-γ (n = 27–28). F. Total numbers of dendritic cells in the brain at day 21 were quantified with the staining of CD45+ CD64- MHCII+ CD11c+ and analyzing their

inflammatory status by CD86 MFI of this population (n = 27–28) G. Quantification of CD45+ CD64- MHCII+ B220- XCR1+ CD172- cDC1s and activation by CD86 MFI determined by flow cytometry. H. Quantification of CD45+ CD64- MHCII+ B220- XCR1- cDC2s and activation by CD86 MFI determined by flow cytometry. I. Quantification of CD45+ CD64- MHCII+ B220- XCR1+ CD172- CD103- cDC1s and activation by CD86 MFI determined by flow cytometry. J. Quantification of CD45+ CD64- MHCII+ B220- XCR1+ CD172- CD103+ cDC1s and activation by CD86 MFI determined by flow cytometry.